Supplemental material for "Anderson mobility gap probed by dynamic coherent backscattering"

L. A. Cobus,[1] S. E. Skipetrov,[2,3] A. Aubry,[4] B. A. van Tiggelen,[2,3] A. Derode,[4] and J. H. Page[1]

[1] *Department of Physics and Astronomy, University of Manitoba, Winnipeg, Manitoba R3T 2N2, Canada*
[2] *Université Grenoble Alpes, LPMMC, F-38000 Grenoble, France*
[3] *CNRS, LPMMC, F-38000 Grenoble, France*
[4] *Institut Langevin, ESPCI ParisTech, CNRS UMR 7587, Université Denis Diderot - Paris 7, 1 rue Jussieu, 75005 Paris, France*

(Dated: April 13, 2016)

This document provides further information on the experimental techniques, the self-consistent theory for backscattered intensity, and the procedure used to fit the predictions of this model to experimental data. Representative values of the best-fit parameters are also presented and discussed.

EXPERIMENTAL METHOD

In this section, we give additional details on the backscattering experiments that we performed to demonstrate a robust new approach for investigating 3D Anderson localization. As emphasized in the letter, time- and angle-resolved backscattering experiments have several important advantages compared with the transmission measurements used in previous studies, enabling investigations of Anderson localization all the way through any mobility gap. Access to the deeply localized regime, where $\xi << L$, obviously requires that the signals emerging from the medium be large enough to be measurable. In transmission, this requirement is difficult, if not impossible, to satisfy. In previous works, transmission through the samples was so greatly reduced inside the transmission dips (where a mobility edge was demonstrated) that measurements were not possible all of the way through the mobility gap, the most deeply localized regime was inaccessible, and the upper mobility edge could not be identified [S1, S2]. By contrast, the reflection geometry that we employ here capitalizes on the distinct advantage that backscattered ultrasound is not affected by this limitation, allowing arbitrarily thick samples to be studied, and a complete investigation of the entire localization regime to be carried out. In addition, backscattering measurements are independent of sample thickness over a significant range of times before the detected signals have been able to reach and travel back from the far side of the sample. This not only simplifies the interpretation of the current backscattering measurements but will also enable future investigations of critical behaviour in which finite size effects can be eliminated. It is these considerations that motivated the design of our backscattering experiments, and have led to the significant progress in the investigation of 3D Anderson localization that is highlighted in the conclusions of our letter.

Given these advantages of backscattering measurements, one might wonder why we have focused on dynamic coherent backscattering rather than near-field detection of the time-dependent transverse intensity profile at the surface of the sample. Such dynamic transverse profile measurements would be expected to give the same type of (absorption-free) information on localization as was obtained previously in transmission [S3], but with all of the additional advantages of the reflection geometry. While this is true in principle, we found that practical limitations preclude effective measurements of this type in reflection. Specifically, near-field measurements in reflection are extremely problematic because the placement of transducers at the sample surface leads to spurious reflections between the generator, sample surface, and detector. In addition, the generation and detection transducers get in the way of each other, making measurements difficult and data for some positions simply inaccessible. We also tried making measurements of the near-field transverse profile through the use of ultrasonic arrays in direct contact with the sample surface, but these were plagued by crosstalk between transducer elements during emission, which interfered with the detection of the interesting signals that have penetrated inside the sample. In addition, placing an array in contact with the sample complicates the boundary conditions. In contrast, coherent backscattering enables the spatial Fourier transform of the entire spatial intensity profile to be measured *in the far-field* with a single ultrasonic transducer array, making it the perfect tool to investigate the growth (or not) of the transverse width in reflection.

The backscattering experiments, as well as the transmission measurements used to corroborate the results for sample L1, were carried out by immersing water-proofed samples and transducers in a large water tank. The pores between the brazed beads in the samples were held under vacuum, thus ensuring that ultrasonic transport inside the sample was confined to the elastic bead network, and that both backscattering and transmission experiments were performed under the same conditions (apart from placement and type of ultrasonic emitters and detectors used). Thus, although both longitudinal and transverse elastic waves are present inside our solid samples, the emitted and measured signals for all experiments have longitudinal polarization (acoustic waves in water).

In backscattering, the response matrix was measured for sample L1 (L2) using 64 (128) elements of a linear ultrasonic array with a central frequency of 1.6 (1.0) MHz, capable of emitting/detecting signals for a frequency range of 0.6 - 1.9 MHz (0.5 - 1.4 MHz). Utmost care was taken to ensure that all possible contributions due to stray background signals were eliminated from the backscattering data by systematically searching for such contributions, removing them where possible, and analysing the data only over the range of times where valid data, uncontaminated by stray signals, were detected. For example, careful placement of the array and sample, the design of a support system for the sample that eliminated spurious reflections, as well as checks with (temporarily inserted) reflecting or opaque objects, were used to ensure that effects from the edges of samples were negligible. The use of short pulses and a large water tank ensured that reflections from the sides of the tank arrived after the backscattered signals from the sample. The data were analyzed only for times greater than 40 μs (to discard any vestiges of specular reflections from the sample surface and single scattering, which might have persisted despite the sophisticated filtering technique that were used to remove these contributions [S4]) and for times less than 200 (120) μs for L1 (L2) (to reject contributions from echoes between the array and sample). Similar care was employed to ensure that only multiply scattered signals from inside the sample were analysed for the transmission measurements on L1 (see Refs. [S1, S2] for details on similar transmission experiments).

For configurational averaging of the backscattering data, the array was translated parallel to the sample, acquiring response matrices at 302 (66) different positions. The distance between the array and sample was 182 (136) mm, so that the backscattering experiments were carried in out in the far field, which for diffuse waves is defined by the condition $a \gg \sqrt{D_B t}$ (a is the sample-array distance, D_B is the Boltzmann diffusion coefficient, t is time). In the diffusive regime (e.g., 1.65 MHz for sample L1), D_B for sample L1 has been measured to be approximately 0.7 mm$^2/\mu$s, and the longest times experimentally available to us are 210 μs, so the approximation of $a = 182$ mm $\gg \sqrt{0.7 \times 210} \approx 12$ mm is valid. In the localized regime, the dynamic spreading of the diffuse halo is less, so that the far-field limit is even better respected.

After filtering the recurrent scattering contribution, the bandwidth-limited time-dependent CBS profiles $R(\theta, t)$ were extracted from the conventional multiple scattering contribution to the response matrix. The dynamic CBS profiles were normalized to eliminate the influence of absorption by dividing $R(\theta, t)$ by $R(0, t)$, since at time t the effect of absorption on the numerator and denominator of this ratio is the same, and therefore cancels. Typical results near the lower mobility edge are shown in Fig. S1, where the data are compared with theoretical predictions as described in the two sections.

SELF-CONSISTENT THEORY FOR DYNAMIC COHERENT BACKSCATTERING

Our theoretical model to describe the dynamic coherent backscattering (CBS) of ultrasound is based on the equations of self-consistent (SC) theory of Anderson localization with a position- and frequency-dependent diffusion coefficient $D(\mathbf{r}, \Omega)$ as derived in Ref. [S5]. In these equations, the scattering mean free path ℓ should be replaced by ℓ_B^* — the transport mean free path in the absence of localization effects — to account for the scattering anisotropy of our samples ($\ell_B^* > \ell$).

To define the mobility edge (ME) and the localization length, we first analyze SC equations in the infinite 3D medium where D becomes independent of position. For the stationary ($\Omega = 0$) diffusion coefficient we obtain

$$D = D_B \left[1 - \frac{3\mu}{(k\ell_B^*)^2}\right], \tag{S1}$$

where D_B is the (Boltzmann) diffusion coefficient in the absence of localization effects and an upper cut-off $q_\perp^{\max} = \mu/\ell_B^*$ (with $\mu \sim 1$) was introduced in the integration over the transverse momentum $q_\perp = \{q_x, q_y\}$ in order to regularize the integral. Here we break the symmetry between $q_\perp$ and q_z to anticipate the experimental geometry of a disordered slab perpendicular to the z axis. A ME of the Anderson transition at $k\ell = (k\ell)_c$ corresponds to $\mu = \frac{1}{3}(k\ell)_c^2(\ell_B^*/\ell)^2$. In the localized regime $k\ell < (k\ell)_c$, an analytic solution of the equations of SC theory can be obtained for a point source emitting a short pulse at $\mathbf{r}' = 0$ and $t' = 0$, in the long-time limit. We obtain an intensity Green's function

$$C(\mathbf{r}, \mathbf{r}', t \to \infty) = \frac{1}{4\pi\xi^2|\mathbf{r} - \mathbf{r}'|} \exp\left(-|\mathbf{r} - \mathbf{r}'|/\xi\right), \tag{S2}$$

where the localization length is

$$\xi = \frac{6\ell}{(k\ell)_c^2}\left(\frac{\ell}{\ell_B^*}\right)\frac{p^2}{1 - p^4}, \tag{S3}$$

and $p = k\ell/(k\ell)_c$. To describe the experimental data, we solve the equations of SC theory in a slab of thickness L with boundary conditions derived in Ref. [S5], where the extrapolation length

$$z_0 = \frac{2}{3}\ell_B^*\frac{1 + R}{1 - R} \tag{S4}$$

depends on the internal reflection coefficient R. To this end, we Fourier transform the SC equations in the transverse plane $\boldsymbol{\rho} = \{x, y\}$ and discretize the remaining ordinary differential equation for $C(q_\perp, z, z', \Omega)$ on a grid for $z \in [0, L]$ [S6]. A sufficiently fine discretization is also introduced for $q_\perp$ and Ω, and the resulting system of linear equations with a tridiagonal matrix of coefficients is

solved numerically using a standard routine `zgtsl` from LAPACK library [S7] for $D(z,\Omega) = D_B$. A new value of $D(z,\Omega)$ is then obtained from the return probability

$$C(\mathbf{r},\mathbf{r}'=\mathbf{r},\Omega) = \frac{1}{2\pi}\int_0^{q_\perp^{\max}} dq_\perp q_\perp C(q_\perp, z, z'=z, \Omega), \quad \text{(S5)}$$

and the solution is iterated until convergence, i.e., $D(z,\Omega)$ does not change by more than a very small amount, typically less than $(5\text{x}10^{-5})\%$, from one iteration to the next. Transmission and reflection coefficients $T(q_\perp,\Omega)$ and $R(q_\perp,\Omega)$ are then calculated as

$$R(q_\perp,\Omega) = D(z,\Omega)\,\frac{\partial}{\partial z} C(q_\perp, z, z'=\ell_B^*, \Omega)\Big|_{z=0} \quad \text{(S6)}$$

and similarly for $T(q_\perp,\Omega)$. We obtain the time-dependent intensity profiles in transmission $T(\boldsymbol{\rho},t)$ and reflection $R(\boldsymbol{\rho},t)$ by a double inverse Fourier transform of $T(q_\perp,\Omega)$ and $R(q_\perp,\Omega)$, respectively. The dynamic CBS profile $R(\theta,t) = R(q_\perp = k_0 \sin\theta, t)$ follows from the observation that the CBS shape is given by the Fourier transform of the 'diffuse intensity halo' at the sample surface [S8].

FITTING SELF-CONSISTENT THEORY TO EXPERIMENTAL BACKSCATTERING DATA

The theory for $R(\theta,t)$ developed in the previous section is valid in the far field, where $\sin\theta = q_\perp/k_0$. Here $k_0 = 2\pi f/v_0$ and $v_0 \approx 1500$ m/s is the speed of sound in water. This is the appropriate limit for comparing with the experimental data, since our backscattering experiments are performed in the far-field (discussed in the first section of this Supplemental Material).

Near the localized regime, backscattered waves may spend a long time in a thick sample without reaching the far side. This means that for a range of times less than twice the typical time for waves to cross the sample, which can be estimated from the peak in the time-dependent transmission, the CBS effect is not sensitive to sample thickness. This is significant because calculations for very thick samples can be prohibitively time-consuming, so the modeling of backscattering in the localized regime is more convenient when there is no explicit dependence on sample thickness. In other words, theory for backscattered waves from a thin sample may also be used for a thicker sample, provided that the range of times investigated is short enough. Here we calculate SC theory for sample L1 and can compare it to experimental CBS profiles of both L1 and L2.

Most input parameters for the calculation of SC theory were determined from measurements performed in separate experiments and could thus be fixed in the fitting procedure. These (fixed) parameters are: scattering mean free path $\ell = 0.9$ mm, reflection coefficient $R = 0.67$, and wave vector $k = 2\pi f/v_p$, with phase velocity $v_p = 2.8$ mm/μs, giving $k\ell = 2.7$ for $f = 1.2$ MHz. The remaining parameter, the transport mean free path $l_B^* = 4$ mm, was determined from SC fitting of transverse confinement (transmission) data from sample L1.

The most important parameter involved in SC theory calculations of $R(\theta,t)$ in the vicinity of an Anderson transition is the localization (correlation) length ξ. As this parameter is unknown a priori, theoretical predictions for $R(\theta,t)$ are calculated for a large range of ξ values from the diffuse/subdiffuse regime to the localized regime (and back again). These values of ξ are determined from $k\ell$ and its critical value at the transition $(k\ell)_c$ using Eq. (S3), with $k\ell$ fixed at the experimentally estimated value for $f = 1.2$ MHz. For each frequency f of experimental data, the experimental CBS matrix $R(\theta,t)$ is fitted with every theory set. All fits are least-squares comparisons between the 2D matrices from experiment and theory, $R(\theta,t)$, using the reduced χ^2 to determine the best-fit values of ξ. All times and θ values are fit simultaneously. This fitting procedure was performed with Wavemetrics software IGOR Pro. By finding the best-fit theory set for each f, the frequency-dependence of the localization (correlation) length $\xi(f)$ was determined. This, in turn, enabled the locations of the two MEs, f_{c1} and f_{c2}, to be determined (these are the frequencies where ξ diverges).

Representative fit results for both samples are shown in Fig. S1, showing the quality of the fits in the subdiffuse regime at a frequency below the first localization transition [Fig. S1(a),(d)], at the first mobility edge [Fig. S1(b),(e)], and in the mobility gap [Fig. S1(c),(f)]. In all cases, the experimental data are well-described by the SC theory: the narrowing of CBS profiles with time is reduced as the ME is reached [Fig. S1(b),(e)], and in the localized regime CBS profiles change even less with time [Fig. S1(c),(f)], with the width approaching a constant at long times.

The Boltzmann diffusion coefficient D_B was a free fit parameter, yielding $D_B(f)$ after the entire fitting process. For sample L1, $D_B \approx 10 \pm 7$ mm$^2\mu$s^{-1} below 1.24 MHz, and $D_B \approx 5 \pm 2$ mm$^2\mu$s^{-1} above 1.24 MHz (from transmission and reflection measurements). The frequency-dependence of $D_B(f)$ is supported by visual inspection of the time-dependence of the transmitted intensity in these regimes, and these values of D_B are similar to the results of previous measurements in similar samples [S2, S3]. For sample L2, the fitting results gave values of D_B ranging from $D_B \sim 13-61$ mm$^2\mu$s^{-1} below 1.24 MHz (peaking in the localized regime) and $D_B \sim 9$ mm$^2\mu$s^{-1} above 1.24 MHz. However, for such a thick sample as L2, the backscattering data are not very sensitive to D_B over the experimentally accessible range of times, so that these estimates for sample L2 are not likely to be very accurate, although they are still consistent with surprisingly large values of D_B, as has been found for other samples in the localized regime. Such values

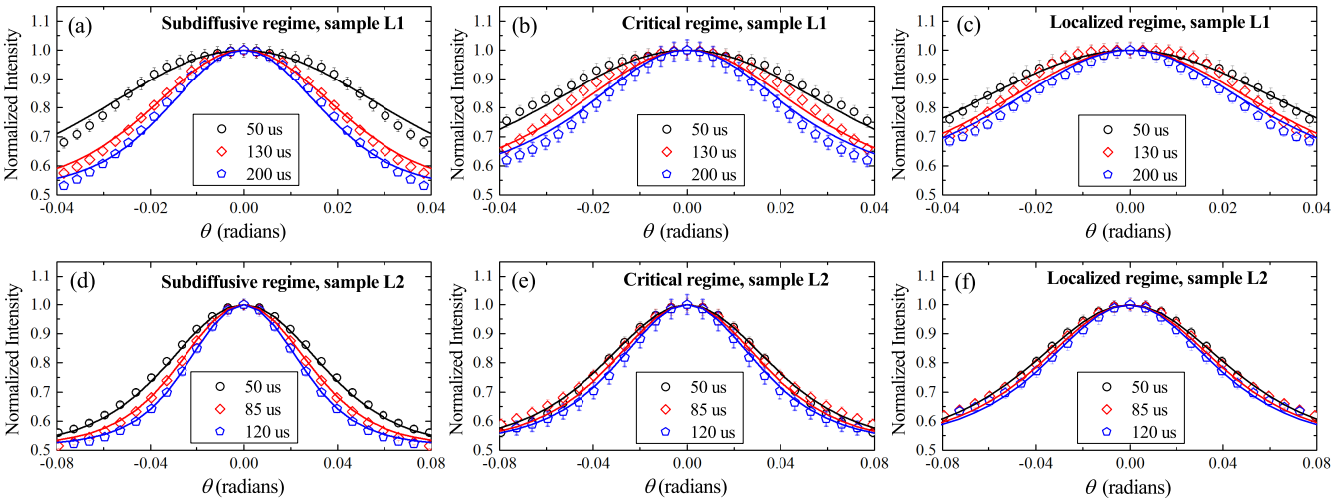

FIG. S1. Self-consistent theory fits (solid lines) to experimental dynamic CBS profiles (symbols). Data shown are from samples L1 (top) and L2 (bottom) for three different times, and for three different frequencies: (a),(d) 1.18 MHz in the subdiffusive regime (correlation length $\xi = 2.1 \pm 0.2$ mm for L1 and 3.2 ± 0.9 mm for L2); (b),(e) near 1.20 MHz at a ME (ξ diverges); and (c),(f) 1.22 MHz in the localized regime ($\xi = 12 \pm 1$ mm for L1 and 16 ± 3 mm for L2). Note that the horizontal scales are different between (a,b,c) and (d,e,f), and that a different range of times is presented. It is also important to note that ξ should not necessarily be the same for both samples at exactly the same frequency.

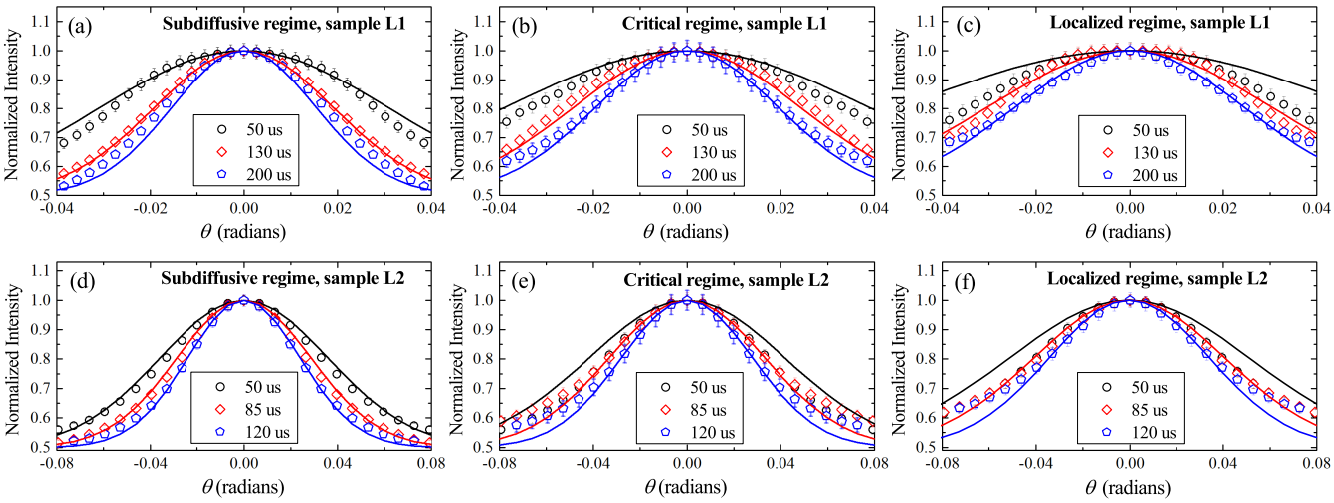

FIG. S2. Diffusion theory fits (solid lines) to experimental dynamic CBS profiles (symbols). Data shown are from samples L1 (top) and L2 (bottom) for three different times, and for three different frequencies: (a),(d) 1.18 MHz in the subdiffusive regime, (b),(e) near 1.20 MHz at a ME; and (c),(f) 1.22 MHz in the localized regime. Since the fits shown in (c),(f) are much worse than those in (a),(d), in Fig. S1(c),(f), and in Fig. 2 of the Letter, it is clear that the diffusion model does not give a satisfactory description of the data in the localization regime.

imply anomalously large values of the energy velocity v_E [S3], motivating future work to seek a theoretical understanding of v_E in the localized regime.

The only other fit parameter was the background intensity level, which was also allowed to vary freely. For both samples L1 and L2, and for almost all frequencies, best fits gave a background of within 10% of the value of 0.5 which would be expected after the removal of the recurrent scattering contribution. This variation of the background intensity results from the challenges of completely removing the recurrent scattering contribution, especially at early times where recurrent scattering dominates the backscattered intensity; by allowing the background intensity to be a free fit parameter, we were able

to ensure that these background fluctuations did not degrade the reliability of our determination of the frequency dependence of the localization (correlation) length.

COMPARISON OF BACKSCATTERING DATA WITH A SIMPLE DIFFUSION MODEL

As has been shown previously (c.f. Figs. 2 and 3 of the Letter), our experimental backscattering data show significant deviations from the behaviour predicted by the diffusion approximation. Since such deviations are often used as 'clues' for where to search for Anderson localization (as they are here), it is of interest to examine the way in which the data diverges from conventional diffusive wave behaviour, and the extent of such effects. Here, we present a simple analysis which shows that our data cannot be described by a theory that assumes a constant diffusion coefficient, and that, in the regime which we have identified as the Anderson localization regime, the self-consistent theory provides a much better description of the data than does the diffusion approximation.

To investigate whether the diffusion approximation can be applied to our data, we fit the experimental CBS profiles $R(\theta,t)$ with a function of the form $R(\theta,t) \propto \exp(-A\theta^2 t)$, where $A \propto D_B$ is a constant factor [S8]. In this model, the CBS profiles must narrow at a constant rate in time, and it is thus not an adequate description of CBS in the localization regime, where the narrowing of dynamic CBS profiles is slowed by the renormalization of diffusion. In the conventional diffusive regime, (1.65 MHz for sample L1), the simple diffusion model fits the data very well at all times (c.f. Fig. 2(a) in the Letter). In the range of frequencies in the mobility gap, as identified by fitting the CBS profiles using the self-consistent theory (see Fig. 4 of the Letter), the diffusion model does not describe the data nearly as well. Representative results for the fitting of this diffusion model to our experimental dynamic CBS profiles are shown in Fig. S2. Clear deviations of the data from conventional diffusion are visible by eye, and are especially evident at larger angles and at later times.

The quality of the theoretical fits to the experimental data can be estimated using the mean squared differences between theory and experiment, i.e., $\chi^2 = \sum_{\theta,t}[R(\theta,t)_{\text{expt}} - R(\theta,t)_{\text{theory}}]^2/N$, where N is the total number of points in $R(\theta,t)$. We define χ^2_{D} for the diffusive model fits to data, and χ^2_{SC} for self-consistent theory fits to data.

First, we compare χ^2_{D} in the conventional diffusion regime ($f_{\text{D}} = 1.65$ MHz) to χ^2_{D} in the entire frequency range studied in this work ($f = 1.17 - 1.27$ MHz), for data from sample L1. These quantities are denoted here by $\chi^2_{\text{D}}(f_{\text{D}})$ and $\chi^2_{\text{D}}(f)$, respectively. We use the ratio of these values to contrast how well the diffusion approximation fits our data in the diffusive regime at f_{D}, compared to the same quantity near and in the mobility gap. Results are shown in the third column of Table S1. For all frequencies, this ratio shows that the fits of the diffusion model to our data near and in the mobility gap are significantly worse than in the diffusive regime. In the mobility gap, the diffusion model performs almost nine times worse than it does in the diffusive regime.

Sample	Frequency range (f)	$\left\langle \frac{\chi^2_{\text{D}}(f)}{\chi^2_{\text{D}}(f_{\text{D}})} \right\rangle_f$	$\left\langle \frac{\chi^2_{\text{D}}(f)}{\chi^2_{\text{SC}}(f)} \right\rangle_f$
L1	outside the mobility gap	2.8	1.3
	inside the mobility gap	8.6	4.0
L2	outside the mobility gap	–	3.2
	inside the mobility gap	–	4.2

TABLE S1. Ratios of χ^2, for samples L1 and L2, as defined in the text of this document. Values are averaged over different frequency ranges (as indicated in Fig. 4 of the main manuscript): (1) outside (but near to) the mobility gap, and (2) inside the mobility gap. Omitted entries are due to the fact that data which exhibit conventional diffusive behaviour are not, at this time, available for sample L2.

Table S1 also compares the goodness-of-fit of diffusion theory to the experimental CBS profiles with that of self-consistent (SC) theory for each sample over the entire frequency range studied in this work. The ratio of χ^2 obtained for diffusion theory fitting to that obtained for SC theory fitting, $\chi^2_{\text{D}}/\chi^2_{\text{SC}}$, matches the trend seen by eye in Fig. S2. From the averages of $\chi^2_{\text{D}}/\chi^2_{\text{SC}}$, we see that the diffusion theory fits are around $1.3 - 3$ times worse than SC theory fits outside the mobility gap, and $3 - 4$ times worse inside the mobility gap. Thus, the SC theory fits are clearly superior to the naïve fits to the simple diffusion approximation for all frequencies investigated, providing additional support for the analysis and conclusions presented in the Letter.

[S1] W. K. Hildebrand, A. Strybulevych, S. E. Skipetrov, B. A. van Tiggelen, and J. H. Page, Phys. Rev. Lett. **112**, 073902 (2014).

[S2] W. K. Hildebrand, *Ultrasonic waves in strongly scattering disordered media: understanding complex systems through statistics and correlations of multiply scattered acoustic and elastic waves*, Doctoral thesis, University of Manitoba (2015).

[S3] H. Hu, A. Strybulevych, J. H. Page, S. E. Skipetrov, and B. A. van Tiggelen, Nat. Phys. **4**, 945 (2008).

[S4] A. Aubry, L. A. Cobus, S. E. Skipetrov, B. A. van Tiggelen, A. Derode, and J. H. Page, Phys. Rev. Lett. **112**, 043903 (2014).

[S5] N. Cherroret and S. E. Skipetrov, Phys. Rev. E **77**, 046608 (2008).

[S6] The actual calculation is performed in dimensionless variables, but we omit this technical detail here for the purpose of clarity.
[S7] Http://www.netlib.org/lapack/.
[S8] E. Akkermans and G. Montambaux, *Mesoscopic Physics of Electrons and Photons* (Cambridge University Press, Cambridge, 2007).